© 2017. Published by The Company of Biologists Ltd | Development (2017) 144, 519-528 doi:10.1242/dev.141390

TECHNIQUES AND RESOURCES

RESEARCH ARTICLE

Genetic mosaics and time-lapse imaging identify functions of histone H3.3 residues in mouse oocytes and embryos

Liquan Zhou‡, Boris Baibakov, Bertram Canagarajah, Bo Xiong* and Jurrien Dean‡

ABSTRACT

During development from oocyte to embryo, genetic programs in mouse germ cells are reshaped by chromatin remodeling to orchestrate the onset of development. Epigenetic modifications of specific amino acid residues of core histones and their isoforms can dramatically alter activation and suppression of gene expression. H3.3 is a histone H3 variant that plays essential roles in mouse oocytes and early embryos, but the functional role of individual amino acid residues has been unclear because of technical hurdles. Here, we describe two strategies that successfully investigated the functions of three individual H3.3 residues in oogenesis, cleavage-stage embryogenesis and early development. We first generated genetic mosaic ovaries and blastocysts with stochastic expression of wild-type or mutant H3.3 alleles and showed dominant negative effects of H3.3R26 and H3.3K27 in modulating oogenesis and partitioning cells to the inner cell mass of the early embryo. Time-lapse imaging assays also revealed the essential roles of H3.3K56 in efficient H2B incorporation and paternal pronuclei formation. Application of these strategies can be extended to investigate roles of additional H3.3 residues and has implications for use in other developmental systems.

KEY WORDS: Histone H3.3, Genetic mosaics, Cell fate decision, Protamine-to-histone exchange

INTRODUCTION

During development from oocyte to embryo, transcriptionally quiescent haploid gametes fuse, and their genomes are remodeled to activate embryonic programs that establish totipotency and subsequent pluripotent cell lineages (Zhou and Dean, 2015). However, the study of chromatin dynamics during this process is technically challenging because of the scarcity of materials and a lack of cell line models. Therefore, proper mouse models to label and perturb chromatin dynamics are particularly useful to understand chromatin reprogramming during this developmental window.

The H3.3 variant is well known for its role in chromatin reprogramming (Jullien et al., 2012) that is antagonized by canonical H3 deposition (Cheloufi et al., 2015; Ishiuchi et al., 2015). H3.3 incorporates into chromatin in a DNA replication-independent manner during the oocyte-to-embryo transition (Akiyama et al., 2011; Torres-Padilla et al., 2006). H3.3 deficiency during oogenesis leads to cell death (Nashun et al., 2015; Tang et al., 2015), ablation in fully grown oocytes inhibits development beyond one-cell (1C) zygotes (Inoue and Zhang, 2014; Lin et al., 2014a) and loss in early embryos both harms genome integrity (Lin et al., 2013) and inhibits pluripotent gene expression (Wen et al., 2014a).

Despite intense investigation, structure-function relationships of specific H3.3 amino acid residues remain unclear in mammals. Manipulation of histone H3-modifying enzymes may perturb non-histone targets and complicate interpretation of epigenetic changes. Greater insight has been obtained by expressing dominant negative mutants of H3.3. For example, H3.3K27R expressed in 1C zygotes results in defective heterochromatin formation and compromises pre-implantation development (Santenard et al., 2010). Studies in glioblastomas identified dominant negative effects of K-to-M mutations in H3.3 (Lewis et al., 2013; Schwartzentruber et al., 2012) and application in early embryos showed that K4 is essential for embryonic genome activation (Aoshima et al., 2015). Additionally, when H3.3 mutants were used to rescue H3.3 knockdown-induced developmental arrest in early embryos, H3.3K36 was shown to inhibit chromatin over-condensation (Lin et al., 2013).

In our study, we developed two strategies and demonstrated their suitability to examine residue-dependent regulation of H3.3 in oogenesis and early embryogenesis, as well as at fertilization. Using a genetic-based mosaic strategy to follow cell fate, we examined oocyte selection in the ovary and blastomere competition in early embryos by stochastically expressing fluorescently tagged exogenous wild-type (WT) or mutant isoforms of H3.3 in individual cells. To study the chromatin-assembling roles of H3.3 at fertilization, we inhibited endogenous H3.3 with morpholinos and rescued expression with morpholino-resistant mutants to test *de novo* nucleosome assembly of the male genome in 1C zygotes.

RESULTS

Genetic mosaic strategy to study specific H3.3 amino acid residues

Expression of the H3.3^{eGFP} transgene was detected in mouse oocytes and embryos derived from H3.3^{eGFP} transgenic mice where expression of the H3.3 transgene was enriched in oocytes relative to ubiquitously expressed nuclear tdTomato fluorescence (Fig. 1A,B). Treatment of transgenic oocytes and embryos with 0.5% Triton X-100 (Hajkova et al., 2010) revealed the association of H3.3^{eGFP} with parental genomes throughout preimplantation development (Fig. S1). To identify functional residues of H3.3 during oogenesis and preimplantation development, we developed a 'genetic mosaic strategy' (Fig. 1C) in which we took advantage of the potential dominant negative effect of H3.3 mutants to generate a transgenic mouse model. The transgenic mouse has a single-copy HISRainbow construct that allowed conditional generation of genetic mosaics stochastically expressing exogenous WT H3.3 or mutant isoforms.

Laboratory of Cellular and Developmental Biology, NIDDK, National Institutes of Health, Bethesda, ML 20892, USA.
*Present address: College of Animal Science and Technology, Nanjing Agricultural University, Nanjing 210095, China.

‡Authors for correspondence (li-quan.zhou@nih.gov; jurrien.dean@nih.gov)

L.Z., 0000-0002-9332-9408; J.D., 0000-0002-7127-0871

Received 21 June 2016; Accepted 7 December 2016

Development (2017) 144, 519-528 doi:10.1242/dev.141390

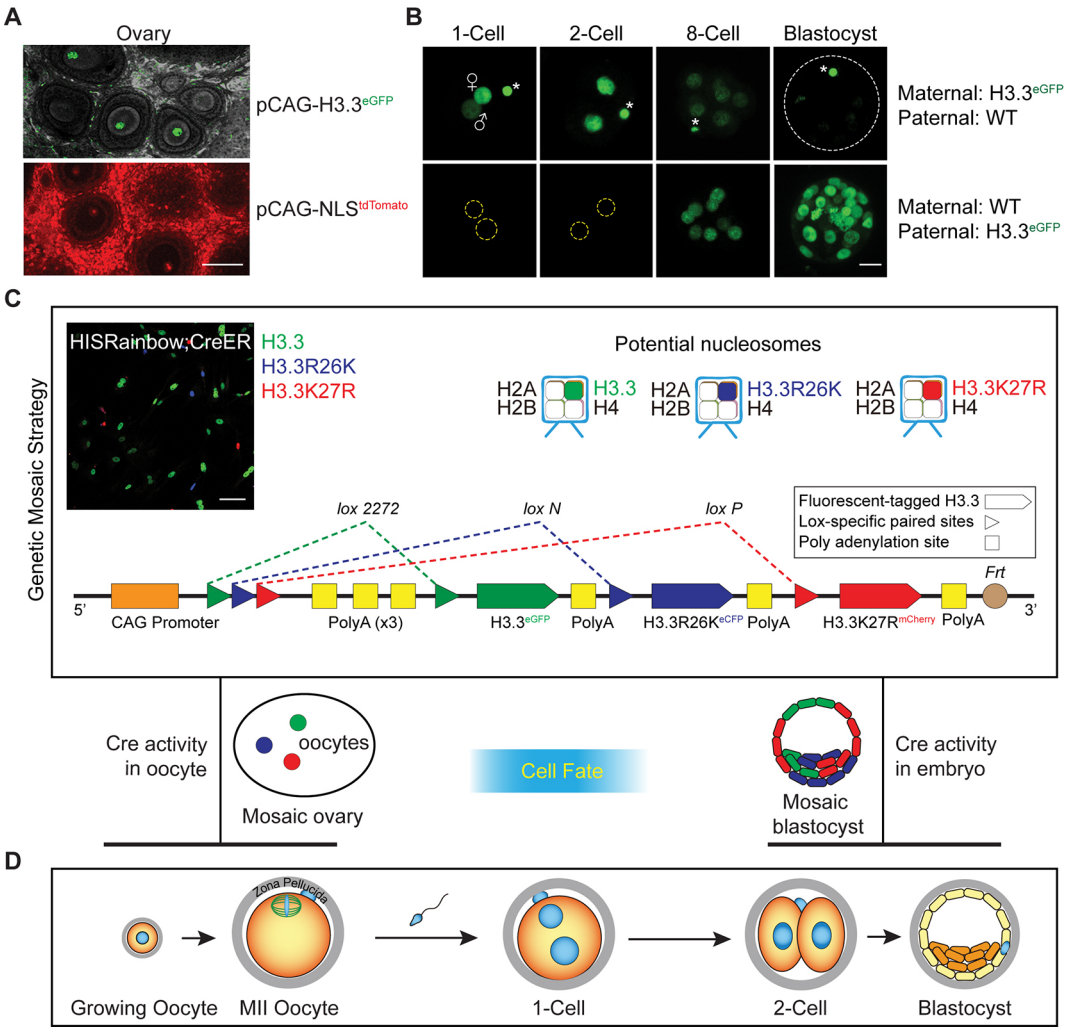

Fig. 1. Experimental scheme of 'genetic mosaic strategy' for studying regulatory roles of H3.3 residues in oocytes and embryos. (A) Confocal (full projection) images of fixed and clarified ovarian sections of H3.3^{eGFP} and NLS^{tdTomato} transgenic mice. Gray background in top image represents autofluorescence. Scale bar: 100 µm. (B) Confocal (full projection) images of early embryos with indicated genotypes expressing fluorescent-tagged histone H3.3 proteins. Asterisk, polar body. Scale bar: 20 µm. (C) In the 'genetic mosaic strategy', transgenic mice carrying the HISRainbow cassette were generated to allow stochastic expression of H3.3 or its mutant isoforms in Cre-expressing cells through mutually exclusive recombination between identical *loxP* sites. Potential nucleosomes after recombination are represented at the top and the feasibility of HISRainbow cassette was verified by inducing Cre activity in HISRainbow; CreER transgenic MEF cells (top left). Scale bar: 100 µm. (D) Scheme of oocyte growth, fertilization and pre-implantation development.

Mating with different Cre-expressing mice produced mosaic ovaries containing genetically different oocytes or mosaic embryos containing genetically different blastomeres. *In vivo* cell-cell competition can thus be traced to identify the functional effects of individual transgenes in oocytes and early embryos (Fig. 1D).

To validate this model, we chose R26 and K27 of H3.3 as candidate residues because of the high abundance of their modifying enzymes in preimplantation development (Tang et al., 2011) (Fig. S2A), their potential roles in transcriptional regulation (Torres-Padilla et al., 2007) and the reported dominant negative effect of the mutant isoforms (Santenard et al., 2010). Three different fluorescent proteins were fused with H3.3 mutants, forming H3.3^{eGFP}, H3.3R26K^{eCFP} and H3.3K27R^{mCherry}, which can be discriminated by confocal microscopy or tag-specific PCR (Table S1). We validated the genetic mosaic strategy by inducing recombination of HISRainbow;CreER with tamoxifen in mouse embryonic fibroblast (MEF) cells followed by quantification with real-time RT-PCR (Fig. S2B). The expression ratio of exogenous H3.3WT, H3.3R26K and H3.3K27R mRNA was ~45:6:1. This ratio was reflected in H3.3 proteins observed by confocal microscopy of the recombined MEF cells (Fig. 1C, top left panel).

Generation of genetic mosaic ovaries reveals that H3.3R26 and H3.3K27 regulate oogenesis

Oogenesis is a developmental program in the ovary that transforms dictyate oocytes within primordial follicles into mature MII eggs (Fig. S3A). The genetic mosaic strategy provides a unique opportunity to study mechanisms that designate oocytes for ovulation (Fig. 2A). Two germline promoters were used to express Cre:*Figla*, which is expressed in resting oocytes (Lin et al., 2014b) and *Zp3*, which is expressed as oocytes begin to grow within a developing follicle (de Vries et al., 2000) (Fig. S3A).

First, MII oocytes from hormonally stimulated HISRainbow; *Figla*-iCre mice were collected to investigate stochastic nuclear fluorescence, indicating successful genetic recombination (Fig. 2B and Fig. S3B). As expected, either single- or dual-color (but not triple-color) fluorescence was detected in ovulated MII oocytes. To test exogenous protein levels generated by the transgenes, we

Development (2017) 144, 519-528 doi:10.1242/dev.141390

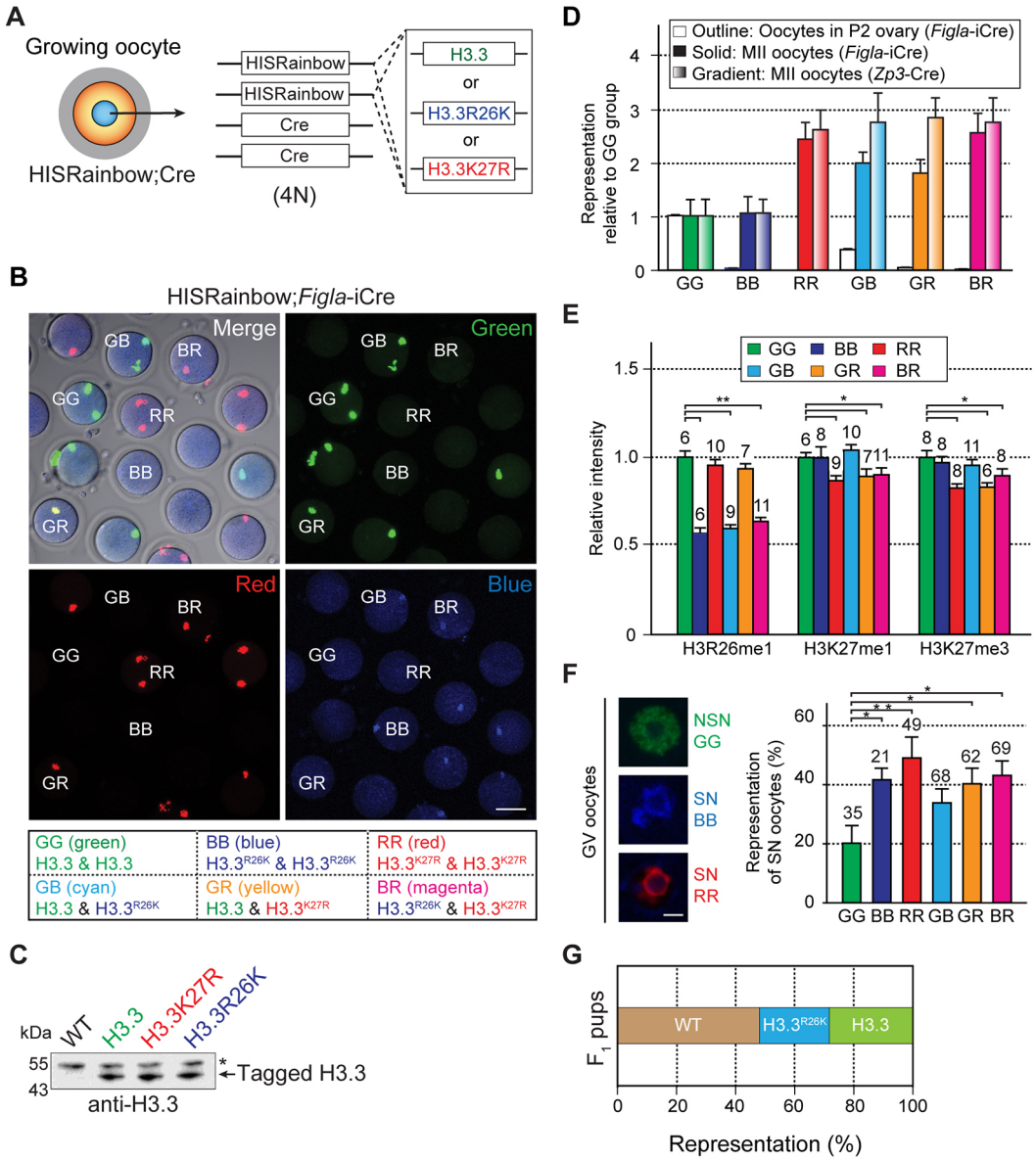

Fig. 2. Dominant negative effect of H3.3R26K or H3.3K27R in oocytes accelerates oogenesis. (A) Scheme of HISRainbow; Cre oocytes with four copies of the chromosomes that express 1-2 alleles of WT and/or H3.3 mutants. (B) Confocal (full projection) and DIC images of MII oocytes isolated from 8- to 12-week-old HISRainbow;*Figla*-iCre mice. Oocytes expressed H3.3^{eGFP} (G), H3.3R26K^{eCFP} (B), or H3.3K27R^{mCherry} (R), from one or two alleles. Scale bar: 50 µm. (C) Immunoblot analysis of HISRainbow; *Figla*-iCre GV oocytes with indicated genotypes for H3.3 expression. 25 oocytes were collected for each group: WT, H3.3^{eGFP} (GG), H3.3K27R^{mCherry} (RR) and H3.3R26K^{eCFP} (BB) and loaded into each lane. Asterisk, non-specific band. Representative gel of two experiments. (D) Relative distribution of H3.3, H3.3R26K and H3.3K27R subpopulations (see also Table S2) in: oocytes in HISRainbow; *Figla*-iCre P2 ovaries (6 replicates); MII oocytes from 8- to 12-week-old HISRainbow; *Figla*-iCre (7 replicates, 191 oocytes); and HISRainbow; *ZP3*-Cre mice (8 replicates, 193 oocytes). Percentage of each subpopulation was normalized to the percentage of oocytes expressing H3.3^{eGFP}, which was set to 1. Mean±s.e.m. (E) Quantification of histone modifications in HISRainbow; *Figla*-iCre oocytes. Mean±s.e.m of $n \geq 6$.; $^{*}p<0.05$, $^{**}p<0.01$. (F) GV oocytes were collected from 3- to 4-week-old HISRainbow; *Figla*-iCre mice, followed by imaging (representative images of indicated genotypes are shown at left) and quantification of NSN and SN configurations (right). Scale bar: 10 µm. Mean±s.e.m. of $n \geq 21$; $^{*}P<0.05$, $^{**}P<0.01$. (G) HISRainbow; *Figla*-iCre females were mated with WT males and pups from the F_1 generation were obtained and genotyped. A total of 24, 12 and 14 pups were obtained from 10 litters with WT, H3.3R26K^{eCFP} and H3.3^{eGFP} genotypes, respectively. No pups with the H3.3K27R^{mCherry} transgene were obtained.

collected single-colored GV oocytes for immunoblot analysis (Fig. 2C and Fig. S3C). The abundance of H3.3 WT, K27R and R26K exogenous isoforms were similar, rendering it unlikely that the observed differences were based on differential histone expression. Similar accumulations of H3.3 WT and mutant exogenous isoforms in oocytes were confirmed by microinjection of cRNAs for quantification of fluorescence intensity (Fig. S3D). Next, we quantified distribution of subpopulations in HISRainbow; *Figla*-iCre oocytes and obtained similar results with HISRainbow;*Zp3*-Cre mice (Fig. 2D, Table S2). This suggested that any change in oocyte subpopulations occurs after primary follicle formation. To obtain initial ratios of transcripts in transgene-expressing cells following genetic recombination, we collected ovaries from postnatal day (P)2 HISRainbow; *Figla*-iCre female for real-time RT-PCR (Table S1, Fig. S3E). We observed that the ratio of H3.3^{eGFP}, H3.3R26K^{eCFP} or H3.3K27R^{mCherry} mRNA is approximately 30:5:1 as detected in the

Development (2017) 144, 519-528 doi:10.1242/dev.141390

recombinant MEF cells. We then compared the predicted distribution of subpopulations based on this ratio in P2 ovaries (Fig. 2D, Table S2). We investigated progressive enrichment of the number of H3.3R26K- and H3.3K27R-expressing oocytes during oogenesis compared with the number of WT H3.3-expressing oocytes. Increases in other subpopulations with expression of two different transgenes showed a dose-dependent, dominant effect of the H3.3 mutants.

Epigenetic modifications in oocytes with amino acid substitutions at R26 and K27 were detected by immunofluorescence (Fig. S3F) and quantified (Fig. 2E). The significant reduction of H3R26 methylation in oocytes expressing H3.3R26K indicated that H3.3R26K has a dominant negative effect. Although statistically significant, there was only a modest reduction in H3K27 methylation in oocytes expressing exogenous H3.3K27R. During oogenesis, oocytes are transformed from an NSN (no Hoechst-positive heterochromatin rim surrounding the nucleolus) to an SN configuration (Hoechst-positive rim surrounding the nucleolus) with significantly reduced transcriptional activity and increased developmental competence. Thus, oocytes collected from HISRainbow; *Figla*-iCre females (Fig. 2F) support a model in which dominant negative effects in oocytes accelerate transcriptional silencing and cause over-representation of the SN configuration in the oocyte pool destined for further maturation and ovulation. To test the developmental competence of these oocytes, we mated HISRainbow; *Figla*-iCre females with WT males. Pups expressing exogenous H3.3 or H3.3R26K were born (Fig. 2G) and, although H3.3K27R-expressing embryos can develop normally to the blastocyst stage (Fig. S3G), no H3.3K27R pups were produced. Therefore, although H3.3R26K-expressed oocytes experienced accelerated oogenesis, they had acquired competence for further development and we did not see obvious developmental abnormalities in these mice after birth.

We also compared the transcriptome of MII oocytes expressing exogenous H3.3, H3.3R26K or H3.3K27R (Fig. 3A). In H3.3R26K oocytes, gene ontology analysis on 2751 significantly upregulated genes (Fig. 3B) suggested that H3.3R26K-involved feedback loop(s) act on chromatin-modifying activity (Fig. 3C). We did not observe enrichment of cell cycle pathway genes within the dysregulated genes, suggesting that cell cycle control is not involved. Surprisingly, only one gene was upregulated in H3.3K27R oocytes (Fig. 3D). This gene encodes L3MBTL2, which assembles a PRC1 family protein complex and may play a key role in the NSN-to-SN transition by transcriptional repression and chromatin compaction. Collectively, development of genetic mosaic ovaries showed that cell competition during oogenesis impacts the pool of ovulated oocytes and this process is regulated by H3.3R26 and H3.3K27.

H3.3K27 influences blastomere contribution to inner cells in genetic mosaic blastocysts

During preimplantation development, totipotent cells differentiate into pluripotent inner or outer cells of the blastocyst that form the embryo and placenta, respectively (Fig. S4A). Blastomere asymmetry starts from the 4-cell (4C) stage (Plachta et al., 2011; Torres-Padilla et al., 2007; White et al., 2016), or even the 2C stage (Biase et al., 2014; Shi et al., 2015), and is regulated by histone-modifying enzymes (Burton et al., 2013; Torres-Padilla et al., 2007). Application of our HISRainbow mouse model provided a non-invasive method to study how H3.3 residues are involved in this cell fate decision.

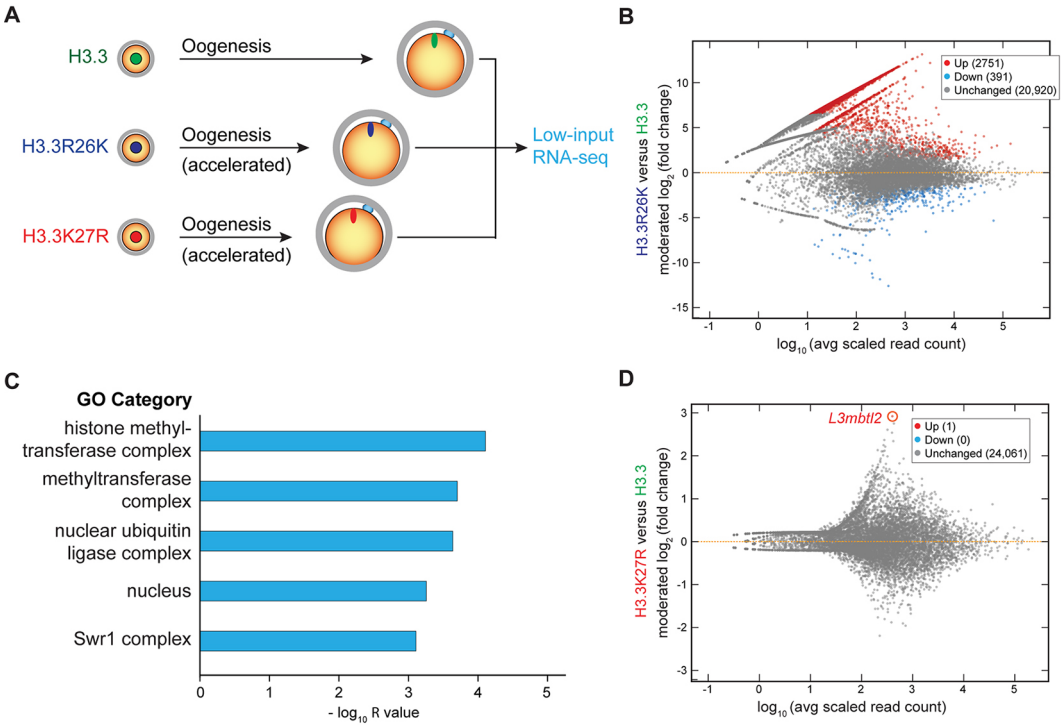

Fig. 3. Transcriptome changes in H3.3R26K- and H3.3K27R-expressing oocytes regulate chromatin silencing. (A) MII oocytes expressing H3.3, H3.3R26K or H3.3K27R were collected from HISRainbow; *Figla*-iCre mice for transcriptome analysis. (B) DESeq2 was used to evaluate differentially expressed transcripts in H3.3R26K-expressing MII oocytes compared with WT H3.3-expressing MII oocytes (adjusted $P<0.05$). MA plot shows $\log_2$ ratio difference of transcripts between MII oocytes expressing H3.3 mutants and those expressing WT H3.3 against the $\log_{10}$ mean average expression. (C) Gene ontology analysis on 2751 upregulated genes in H3.3R26K-expressing MII oocytes. (D) MA plot shows differentially expressed transcripts in H3.3K27R-expressing MII oocytes compared with WT H3.3-expressing MII oocytes (adjusted $P<0.05$). Upregulated *L3mbtl2* gene is highlighted and labeled.

Development (2017) 144, 519-528 doi:10.1242/dev.141390

To acquire early mosaic mouse embryos, we mated HISRainbow males with CreER female mice to obtain double transgenic early embryos and induced genetic recombination (Fig. 4A). This resulted in stochastic expression of WT or mutant H3.3 transgenes in individual blastomeres. Early blastocysts were then collected to identify contributions of blastomeres expressing different exogenous proteins (Fig. 4B). Generally, ∼10% of H3.3^{eGFP}-expressing blastocysts had a H3.3K27R^{mCherry} signal that was consistent with the recombination efficiency of the HISRainbow cassette (Fig. S2B). For quantification, we collected and imaged 30 blastocysts in which H3.3^{eGFP} and H3.3K27R^{mCherry} were clearly and exclusively expressed in individual blastomeres. Unexpectedly, the H3.3R26K^{eCFP} signal was not observed in all 30 blastocysts. This suggests either death of H3.3R26K-expressed cells or elimination of H3.3R26K proteins during preimplantation development. Therefore, we collected GV oocytes from H3.3R26K transgenic females (Fig. 2G) and mated the transgenic females with WT males to acquire early embryos. We observed a strong signal of H3.3R26K in oocytes, but only a faint signal in early embryos (Fig. S4B), which suggested that exogenous H3.3R26K protein accumulated during oogenesis is eliminated during early embryogenesis. This may also explain why transgenic H3.3R26K mice, but not H3.3K27R mice, were viable despite the potential dominant negative effect of both transgenes. Similar behavior was reported for macroH2A protein (Chang et al., 2005), which accumulates in oocytes, but is eliminated after fertilization.

To illustrate the possible impact of exogenous H3.3K27R on inner cell contribution, we reconstructed blastocysts to identify blastomere localization and used CDX2 staining to identify outer cells (Fig. 4C). We further determined total cell numbers according to blastomere localization (inner or outer) and nuclear fluorescence (Fig. 4D, Table S3). Our results showed that ectopic expression of H3.3K27R in blastomeres leads to an increased contribution to the outer cells and a corresponding decreased contribution to the inner cells. To identify potential mechanisms involved in this process, we probed for H3K27 methylation in early mosaic blastocysts, and confirmed the dominant negative effect of the H3.3K27R mutant in blastomeres (Fig. 4E). Change of cell fate allocation by exogenous H3.3K27R expression may be simply explained by delayed developmental progress through cell cycle regulation. To test this possibility, we obtained 18 recombined mosaic embryonic cells as early as the 8- to 16-cell stage to obtain initial ratios of transgene-expressing cells following genetic recombination (Fig. S4C, Table S4). Again, no H3.3R26K^{eCFP} signal was detectable in these embryos. We summarized total cell numbers expressing either exogenous H3.3WT or H3.3K27R and found that the initial ratio was ∼3.0, which was very similar to the ∼3.3 ratio observed in mosaic blastocysts. The ratio is lower than what we observed in MEF cells (Fig. S2B) and P2 ovaries (Fig. S3E) because only embryos expressing both H3.3 and H3.3K27R exogenous proteins were imaged for quantification. This result identified similar developmental progress of H3.3WT and H3.3K27R blastomeres. OCT4 (POU5F1) is a master transcriptional regulator of inner cell lineage and has comparable expression in all blastomeres at the early blastocyst stage. We found that H3.3K27R expression reduced OCT4 protein level with a corresponding reduced contribution of

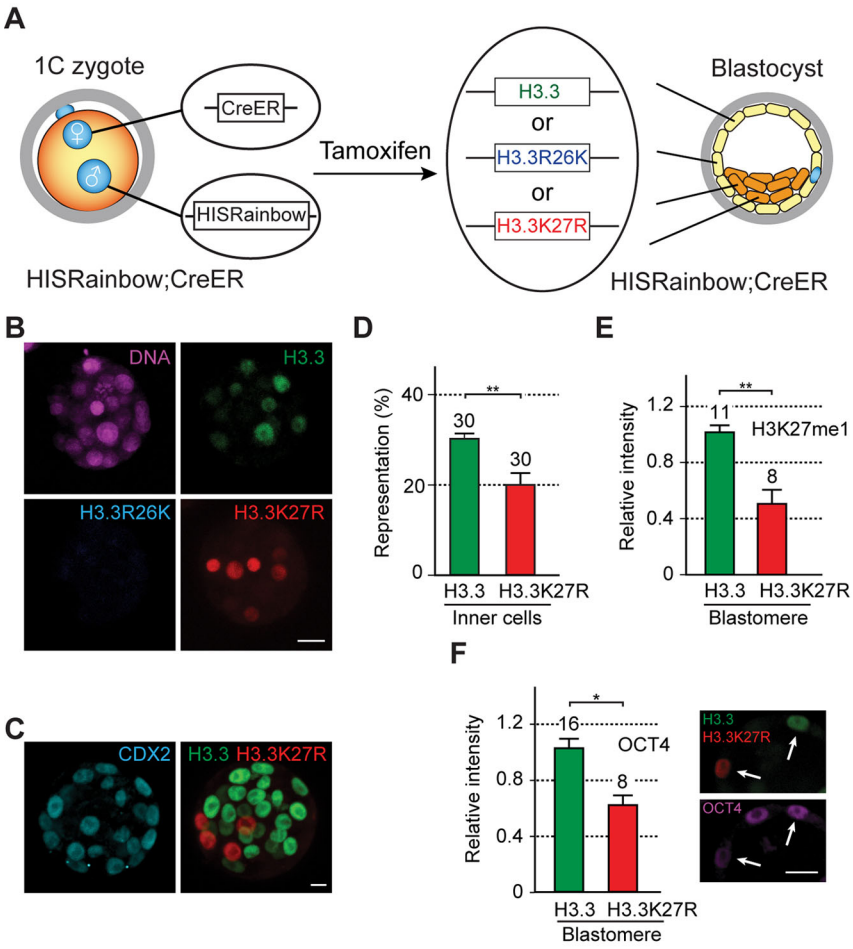

Fig. 4. H3.3K27 regulates the first cell lineage specification. (A) To generate mosaic blastocysts, HISRainbow male mice were mated with CreER female mice to obtain 1C zygotes. Early 4C embryos were collected and treated with 0.2 µM 4-hydroxytamoxifen for 12 h. This led to nuclear import of the Cre enzyme and genetic recombination within the HISRainbow construct. Embryos were further cultured to early blastocysts for examination. (B) Representative confocal (full projection) images of mosaic blastocysts with individual blastomeres expressing either H3.3^{eGFP} or H3.3K27R^{mCherry}. DNA was stained with DRAQ5. Scale bar: 10 µm. (C) Representative confocal (full projection) images of mosaic blastocysts stained with anti-CDX2 antibody. Scale bar: 10 µm. (D) Quantification of H3.3^{eGFP}- and H3.3K27R^{mCherry}-expressing blastomeres in the inner cells of early blastocysts. Mean±s.e.m. of 30 blastocysts; $^{**}P<0.01$. (E) Immunofluorescence with anti-H3K27me1 antibody of cells expressing WT H3.3 (n=11) and H3.3K27R (n=8). Mean±s.e.m.; $^{**}P<0.01$. (F) Immunofluorescence with anti-OCT4 of cells expressing WT H3.3 (n=16) and H3.3K27R (n=8). Arrows indicate co-expression of OCT4 in H3.3- and H3.3K27R-expressing cells. Mean±s.e.m.; $^{*}P<0.05$. Scale bar: 20 µm.

Development (2017) 144, 519-528 doi:10.1242/dev.141390

H3.3K27R-expressing cells to the inner cell population (Fig. 4F). The ability to determine a regulatory role of H3.3K27 on the first cell fate decision in a non-invasive manner illustrates the utility of establishing genetic mosaic blastocysts.

Mutant rescue strategy to study H3.3 residues in zygotes

Zygotes are totipotent cells with unique chromatin structures (Bošković et al., 2014; Macfarlan et al., 2012). During formation of early embryos, the most striking chromatin event is repackaging the male genome in zygotes through protamine-to-histone exchange. This process is disrupted by inhibiting endogenous H3.3 or its chaperone HIRA (Inoue and Zhang, 2014; Lin et al., 2014a). To study chromatin dynamics in zygotes, we established a time-lapse imaging assay (Fig. S5A) and monitored developmental events following fertilization (Fig. 5A), including zinc sparks induced by sperm-egg fusion (Fig. S5B) and protamine-to-histone exchange (Fig. S5C). Specifically, we determined that histone variant H3.3, together with H2A.X and macroH2A (mH2A) are incorporated into the male genome (Fig. S5D,E).

With this assay, we could employ a 'mutant rescue strategy' (Fig. 5B) to examine how H3.3 residues were involved in 1C zygote formation (Fig. 5C). First, morpholinos were used to inhibit endogenous H3.3 translation in GV oocytes. Then, morpholino-resistant mutant H3.3 (cRNA from *Drosophila melanogaster*) was co-expressed in oocytes that were then matured *in vitro* and fertilized to study the reassembly of male chromatin structures. This strategy makes it feasible to explore the developmental role of any H3.3 residues during cleavage-stage embryogenesis while avoiding any adverse effect that might disrupt oogenesis.

H3.3K56A-rescued zygotes fail to form male pronuclei

To study maternally stored H3.3 during male pronucleus formation, we cultured full-grown GV oocytes for *in vitro* fertilization (Fig. 6A). Time-lapse imaging was performed to monitor individual steps (Fig. S6A). Under these experimental conditions, ~70% of oocytes (120 oocytes examined) progressed and formed 1C zygotes with two pronuclei. The remainder either did not mature or were not fertilized and were excluded from analysis. We first injected morpholinos directed against GFP to test whether injection influenced development and found that more than 80% of fertilized oocytes formed two pronuclei (Fig. S6B). We then targeted H3.3 with injected morpholinos to prevent translation of endogenous H3.3A and H3.3B, and observed impaired formation of the male pronucleus in zygotes (Fig. 6B and Fig. S6C) as previously reported (Inoue and Zhang, 2014; Lin et al., 2014a). This phenotype could be rescued by co-injection of cRNA encoding H3.3 (Fig. 6B and Fig. S6C) but not H3.1 (Fig. S6B), a canonical histone that does not incorporate into the male genome after fertilization (Fig. S5D,E).

To further identify how H3.3 residues regulated male pronucleus formation we turned to H3.3K56, which is positioned at the entry-exit point for DNA on nucleosomes and may regulate nucleosome stability (Hyland et al., 2005). In mice, H3K56 acetylation first appears in parental genomes when pronuclei start to form and increase their volume (Ziegler-Birling et al., 2016). We tested K-to-A and K-to-R mutations at H3.3K56 for their ability to rescue the H3.3-depleted phenotype. Both K56A and K56R mutants were inefficient in supporting male pronuclei formation (Fig. 6B and Fig. S6B) and we focused on the K-to-A mutant for the following experiments. Failure of the H3.3K56A mutant to rescue pronuclei formation was not due to poor quality of injected cRNA because the male genome volume in H3.3K56A-rescued zygotes resembled normal re-condensation rather than normal de-condensation (Fig. 6C) in contrast to changes in nuclear areas quantified in H3.3-deficient zygotes. We also stained lamin B in morpholino-treated zygotes without and with rescue by H3.3 WT or H3.3K56A cRNA (Fig. 6D). We observed that neither morpholino-treated nor H3.3K56A-rescued zygotes formed nuclear membranes surrounding the male genome, in contrast to H3.3WT-rescued zygotes. Severely impaired nuclear membrane formation leads to failure of nuclear factor import necessary for organization of the male genome. To robustly monitor histone H2B binding, we performed the rescue assay with $H2B^{mCherry}$ transgenic oocytes. When H3.3K56A cRNA was used for injection, H2B incorporation (which reflects nucleosome formation), was significantly reduced in the male genome (Fig. 6E). We therefore propose that sufficient nucleosome density is important for nuclear membrane assembly and that male pronuclear formation is a process that depends on H3.3K56.

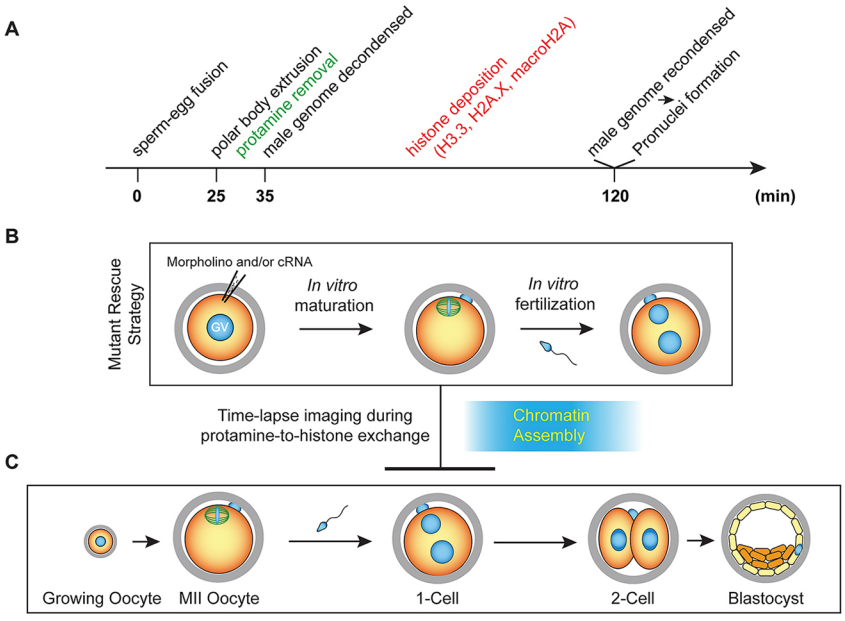

Fig. 5. Experimental scheme of 'mutant rescue strategy' for studying regulatory roles of H3.3 residues in mouse zygotes. (A) Scheme of developmental events during parental genome reorganization based on time-lapse imaging analysis following fertilization. Protamine removal and histone deposition are highlighted in green and red, respectively. Pronuclei are formed immediately after the male genome is re-condensed. (B) In the 'mutant rescue strategy', morpholinos targeting endogenous H3.3A and H3.3B are injected into full-grown GV oocytes that are then matured and fertilized *in vitro* to form a 1C zygote with deficient H3.3 proteins. Morpholino-resistant cRNAs expressing H3.3 mutants are co-injected to study the roles of residue candidates by time-lapse confocal microscopic imaging. (C) Scheme of oocyte growth, fertilization and pre-implantation development.

Development (2017) 144, 519-528 doi:10.1242/dev.141390

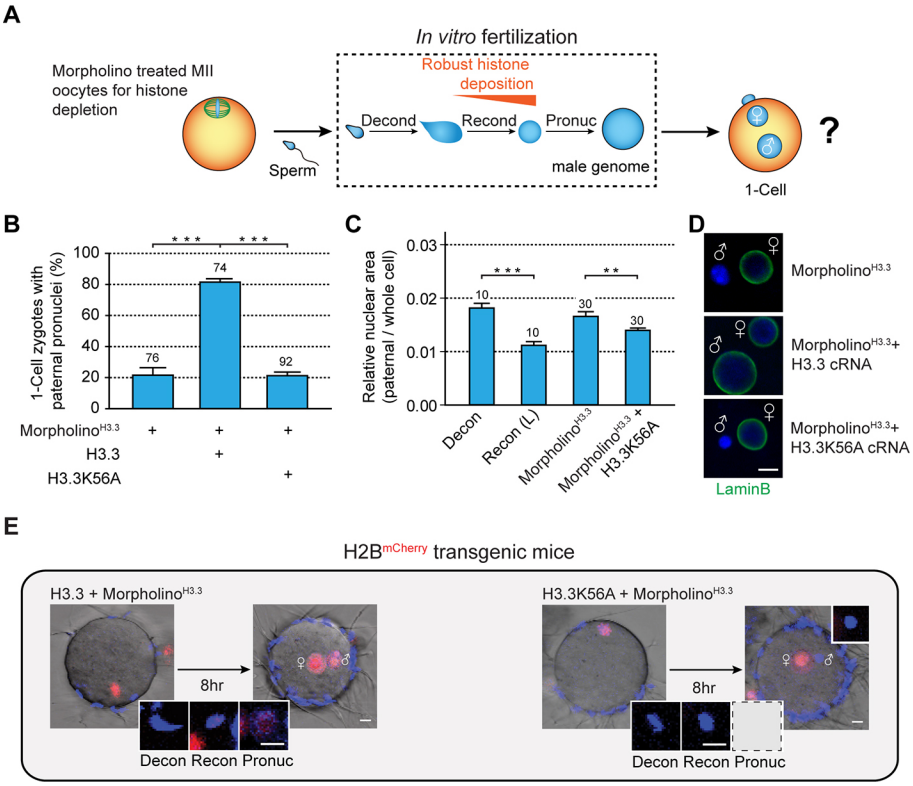

Fig. 6. H3.3K56 is essential for male pronuclei formation. (A) Parental genomes can be imaged during fertilization to monitor their dynamics. Translation of endogenous H3.3 can be inhibited by morpholinos to examine morphological changes of genomes. (B) Formation of paternal pronuclei determined morphologically and quantified. Mean± s.e.m. of 74-92 zygotes. (C) Relative nuclear areas calculated for the male genome. Nuclear areas from de-condensed genome (Decon) and late re-condensed genome (Recon L) were obtained from live imaging after normal sperm-oocyte fusion. For zygotes derived from GV oocytes injected as indicated, only those without paternal pronuclei were used for quantification. Mean±s.e.m. of 10-30 zygotes. ***P*<0.01, ****P*<0.001. (D) Immunostaining of lamin B in endogenous H3.3-deficient zygotes without (top, *n*=16) or with H3.3 WT (middle, *n*=15) or H3.3K56A (bottom, *n*=22) cRNA rescue. Zygotes were imaged for each group with a representative image displayed. Scale bar: 10 µm. (E) H2B^{mCherry} transgenic GV oocytes were injected with morpholinos and cRNA encoding WT H3.3 (top, representative image of 10 zygotes) or H3.3K56A (bottom, representative image of 8 zygotes), followed by maturation and live imaging for fertilization. Scale bars: 10 µm.

DISCUSSION

In our study, we present two approaches showing that disturbance of specific amino acid residues of H3.3 (instead of ablation of the whole H3.3 protein) activates divergent H3.3 functions to support oogenesis and early development. Through mosaic mouse models expressing fluorescently tagged histones, we stochastically inhibited H3.3 modifications and demonstrated that cell-cell competition involving histones exists between both germ and embryonic cells. Our imaging system allowed us to study reorganization of the male-derived genome following fertilization and we show that H3.3 regulates *de novo* chromatin assembly in a residue-dependent manner.

Successful application of our two approaches provides useful information for how H3.3 regulates mouse oocyte and embryo development in a residue-dependent manner. H3.3 differs from canonical H3 by four to five amino acid residues. This alteration affects partners that interact with H3 proteins and determines unique chromatin incorporation of H3.3 (Liu et al., 2012) that modulates nucleosome structures (Jin and Felsenfeld, 2007) to regulate chromatin dynamics. Although it remains unclear whether H3.3 has unique modifications compared with canonical H3, specific 'reader' proteins recognizing H3.3 modifications have been shown to mediate activities involving H3.3. ZMYND11 (BS69) contains tandemly arranged chromatin-recognition modules and specifically binds to trimethylated H3.3K36 (Guo et al., 2014; Wen et al., 2014b). ZMYND11 co-occupies active genes with H3.3 and regulates both transcription elongation and intron retention. Whether other H3.3-specific writers, readers and erasers exist and whether their loss in oocytes or embryos results in phenotypes similar to that caused by the H3.3 mutations provide questions for future studies. In addition to recruitment of histone-modification readers that regulate the epigenetic landscape, crosstalk among histone modifications plays an important role in controlling gene expression. The most common examples for histone modification crosstalk are between modifications on the same histone tail, such as the antagonism between H3R2 and H3K4 (Hyllus et al., 2007). Trans-histone crosstalk is also observed, and H4K44 is essential for H3K36 methylation (Du et al., 2008). In rare cases, histone modifications may also trigger cleavage of H3 tails by proteases (Duncan et al., 2008). Although we did not detect crosstalk between H3.3R26 and H3.3K27 modifications in this study, it is likely that this model system will be useful to investigate such interactions and their subsequent effect on development.

Our genetic mosaic model and histone rescue assay establish a framework for investigating chromatin dynamics during oogenesis, fertilization and pre-implantation development. In recent years, application of high-throughput sequencing technologies in oocytes (Stewart et al., 2015) and early embryos (Dahl et al., 2016; Liu et al., 2016; Lu et al., 2016; Wu et al., 2016) has improved our understanding of the epigenetic landscape and has led to greater insight into molecular mechanisms of chromatin reorganization. The combination of these sequencing technologies and our new techniques will facilitate exploration of regulatory networks to identify key chromatin modulators and determine their importance in the oocyte-to-embryo transition.

MATERIALS AND METHODS

Unless otherwise noted, chemicals and other reagents were obtained from Sigma-Aldrich. Restriction enzymes were obtained from New England BioLabs. All animal studies were performed in accordance with guidelines of the Animal Care and Use Committee of the National Institutes of Health under a Division of Intramural Research, NIDDK approved animal study protocol.

Mice

To establish pCAG-H3.3^{eGFP} transgenic mice, the H3.3^{eGFP} fragment from H3.3-pEGFP-N1 (gift from Dr Philippe Collas; Delbarre et al., 2010) was subcloned into pCAGEN. To produce ZP3-H2B^{mCherry} transgenic mice, the 1.6 kb ZP3 promoter (Svoboda et al., 2001) and H2B cDNA cloned from mouse ovary RNA were inserted into pmCherry-N1. The HISRainbow

Development (2017) 144, 519-528 doi:10.1242/dev.141390

construct was generated by sequentially ligating lox 2272+lox N+lox P, polyA×3+lox 2272, H3.3-eGFP, polyA+lox N, H3.3^{R26K}-eCFP, polyA+lox P, H3.3^{K27R}-mCherry, polyA+frt (all with 5′ *Xba*I restriction sites and 3′ *Nhe*I or *Eco*RI restriction sites) into the pCAGEN plasmid (Addgene) (Rinkevich et al., 2011). After digestion with *Spe*I and *Eco*RI, the transgene was gel-purified and injected into the male pronucleus (Avella et al., 2014). These mice were then crossed with Flpe-Cre transgenic mice (Jackson Laboratory) for several generations until only one copy of transgene was detected in the mouse line. Platinum Blue PCR SuperMix (Thermo Fisher Scientific) was used for genotyping and primer sequences are listed in Table S1. PCR cycling conditions were 94°C for 2 min followed by 32 cycles of 94°C for 30 s, 58°C for 30 s, 72°C for 30 s, and a final extension step of 72°C for 5 min.

Figla-iCre transgenic mice were from our colony (Lin et al., 2014b); *ROSA*$^{nT\text{-}nG}$ (pCAG-NLS^{tdTomato}), ZP3-Cre and CAG-CreER transgenic mice were obtained from the Jackson Laboratory; *Prm1*-eGFP transgenic mice were a gift from Dr Pawel Pelczar (Haueter et al., 2010). To test for fertility, female mice were co-caged with WT fertile males. To collect HISRainbow;CreER MEF cells, HISRainbow male mice were mated with CreER female mice. Embryos from plugged female mice were harvested at embryonic day (E) 13.5 to obtain MEF cells (http://web.mit.edu/jacks-lab/protocols/Making_MEFs_tables.html). To induce recombination in MEF cells, 1 µM 4-hydroxytamoxifen was used.

Oocyte and embryo culture

Female mice were primed with eCG (5 IU) and full-grown oocytes were collected 48 h later by ovarian puncture. Healthy-looking oocytes were cultured in α-MEM (ThermoFisher Scientific) supplemented with 3 mg ml^{-1} BSA (MP Biomedicals), 10 ng ml^{-1} EGF (Corning) and 2.5 µM milrinone. For *in vitro* maturation, milrinone was omitted and oocytes were incubated for 16-18 h. To obtain MII oocytes or preimplantation embryos, female mice were stimulated with hCG and mated with males when embryos were needed (Zheng and Dean, 2009). 1C zygotes were collected from oviducts and cultured in KSOM (Zenith Biotech) supplemented with 4 mg ml^{-1} BSA at 37°C for further development. To induce recombination, early 4C embryos of HISRainbow;CreER mice were cultured in KSOM with 0.2 µM 4-hydroxytamoxifen (Tabansky et al., 2013) for 12 h, transferred to KSOM alone and incubated until the early blastocyst stage (equivalent to E3.5).

Oocyte and embryo microinjection

Endogenous mouse H3.3 is encoded by *H3f3a* (Chr 1) and *H3f3b* (Chr 11), which are translated into identical proteins. All H3.3 related constructs in the study were cloned from the H3.3-pEGFP-N1 (gift from Dr Philippe Collas) (Delbarre et al., 2010) expressing H3.3 of *D. melanogaster*, which has the same amino acid sequence as the mouse protein. The macroH2A-GFP plasmid was obtained from Addgene (plasmid 30515). Other cDNA constructs were generated from mouse ovary RNA and subcloned into pcDNA3.1/myc-his (Thermo Fisher Scientific). T7/T3 polymerase was used for *in vitro* mRNA synthesis [mMessage mMachine Kit, poly(A) tailing kit; Thermo Fisher Scientific] and an Eppendorf FemtoJet Microinjector was used for oocyte/embryo microinjection with pulsed-flow. 1-2 pl *in vitro* transcribed cRNA and/or morpholinos (MO) (Gene Tools) were injected into the cytoplasm of oocytes in M2 medium (Zenith Biotech) supplemented with 4 mg ml^{-1} BSA. In these experiments, cRNA encoding histones [100 ng µl^{-1} for histone tracking to avoid intra-S-phase checkpoint activation (Santenard et al., 2010); 500 ng µl^{-1} for normal/mutant H3.3 rescue in absence of endogenous H3.3 proteins] and 0.5 mM of morpholinos against H3.3A (AAGGACACCTCCTTACTTACCCCCC) and H3.3B (CGGGCCATTTTTTTTCACCCAAAGC) were used. Morpholino against GFP (0.5 mM) (ACAGCTCCTCGCCCTTGCTCACCAT) was used to test the impact of injection on development. To promote germinal vesicle breakdown and *in vitro* maturation, oocytes were cultured at 37°C for 4-8 h after microinjection before transfer to milrinone-free medium.

Isolation of genomic DNA, RNA and real-time PCR

To isolate genomic DNA, cells were lysed (100 mM Tris-HCl, pH 8, 200 mM NaCl, 5 mM EDTA, 0.2% SDS) at 37°C for 16 h and DNA was precipitated by isopropanol. RNeasy Mini Kit (Qiagen) was used to isolate total RNA. SuperScript III First-Strand Synthesis System (Thermo Fisher Scientific) was used for reverse transcription. iTaq Universal SYBR Green Supermix (Bio-Rad) was used for real-time PCR to assess primer efficiency and transcript abundance.

Expression of the three transgenes (H3.3^{eGFP}, H3.3R26K^{eCFP} and H3.3K27R^{mCherry}) from the HISRainbow cassette was quantified to determine recombination efficiency. For HISRainbow;CreER MEF cells, Cre activity was induced by 4-hydroxytamoxifen for 48 h, then RT-PCR was performed to determine gene expression using tag-specific primer pairs for eGFP, eCFP and mCherry. Primer efficiency was normalized by PCR amplification using untreated HISRainbow;CreER MEF genomic DNA. In HISRainbow; *Figla*-iCre ovaries, eGFP is expressed by the *Figla* promoter. Therefore, the H33XFPUTR primer pair was used for pre-amplification of transcripts from HISRainbow cassette, and purified PCR product provided a template for quantification using tag-specific primer pairs. Primer sequences are listed in Table S1.

Preparation of transparent mouse ovaries

After isolation, ovaries were fixed overnight in 4% paraformaldehyde (Electron Microscopy Sciences), washed three times in PBS and clarified in prepared ScaleA2 solution (Hama et al., 2011) for 2 weeks. Using a LSM 780 confocal microscope, single-channel confocal (single projection) images were obtained with background tissue autofluorescence.

Immunofluorescence and confocal microscopy

Oocytes/embryos were fixed and permeabilized with 3.7% paraformaldehyde and 0.5% Triton X-100 in PBS containing 0.3% polyvinylpyrrolidone for 40 min and blocked for 30 min at room temperature with SuperBlock Blocking Buffer in PBS containing 0.05% Tween-20 (Thermo Fisher Scientific). Oocytes/embryos then were incubated with primary antibody (diluted 1:100 in SuperBlock Blocking Buffer containing 0.05% Tween-20) overnight at 4°C and then secondary antibody for 2 h at room temperature. Confocal and DIC images (63×/1.2 NA water immersion objective) were exported as full-resolution TIFF files and Zeiss Microscope Software was used for quantification. For imaging of HISRainbow;CreER blastocysts, embryos were fixed and incubated with 10 µM DRAQ5 (Alexis Biochemicals) for DNA labeling, and 2 µm confocal sections were obtained. NIH ImageJ was used for three-dimensional embryo reconstruction.

Immunoblot

Immunoblots were performed as previous described (Burkart et al., 2012). Generally, oocytes were freshly collected and lysed in Tris-glycine SDS loading buffer with 4% β-mercaptoethanol, separated on 4-20% Tris-glycine gradient gels (Invitrogen), probed by primary antibody overnight at 4°C and secondary antibody conjugated to HRP 1 h at room temperature.

Antibodies

The following primary antibodies were used for immunofluorescence: H3K27me1 (Active Motif, 39377, 1:100), H3K27me3 (Abcam, ab6147, 1:100), H3R26me1 (Abcam, ab130898, 1:100), OCT4 (Active Motif, 39811, 1:100), CDX2 (BioGenex, Clone CDX2-88, 1:200) and laminB (Santa Cruz, sc-6217, 1:150). H3.3 (Millipore, 17-10245, 1:800) antibody was used for immunoblot. Secondary antibodies for immunofluorescence (Thermo Fisher Scientific) or immunoblot (Santa Cruz) were used according to the manufacturer's instructions.

In vitro fertilization and time-lapse imaging

The zona pellucida was removed from MII oocytes by acid Tyrode's solution and sperm were capacitated in human tubal fluid (HTF) (Zenith Biotech) supplemented with 4 mg ml^{-1} BSA. Zona-free MII oocytes were transferred into HTF followed by the addition of capacitated sperm at low concentrations (1×10^4-5×10^4 ml^{-1}). Sperm parameters (count, motility and morphology) were determined by computer-assisted sperm analysis (CASA-IVOS, Hamilton Thorne Biosciences). For time-lapse imaging of sperm-oocyte fusion, a glass-bottomed dish (MatTek Corporation) was

Development (2017) 144, 519-528 doi:10.1242/dev.141390

pretreated with a solution of poly-lysine for 30 min at room temperature, filled with 4 ml of HTF supplemented with 4 mg ml^{-1} BSA and incubated in a humidified chamber at 37°C. Zona-free MII oocytes were immobilized at the bottom of the dish, inseminated with capacitated sperm and imaged by a LSM 780 (Carl Zeiss) confocal microscope (20× objective; time intervals, 5-6 min; optical sections, 7 µm). To monitor morphological changes, 20 ng ml^{-1} Hoechst 33342 was used to label DNA. To image zinc sparks, 20 µM FluoZin-3 (ThermoFisher Scientific) was added (Kim et al., 2011; Que et al., 2015) and images were obtained at 10 s intervals over 5 h with a maximum pinhole.

RNA-seq and bioinformatics analysis

The SMARTer Ultra Low RNA Kit (Clontech) was used for cDNA synthesis and Nextera DNA Sample Preparation Kit (Illumina) was used for library preparation according to the manufacturers' protocols. Libraries were analyzed by the Agilent High Sensitivity DNA Kit for proper quantity and size distribution. PicoGreen was used for DNA quantification before sequencing. Two biological replicates were prepared for each group and samples were sequenced on an Illumina HiSeq 2000 as single-end 50 bp reads in the NIDDK Genomics Core. The RNA-seq dataset in this study has been deposited in the Gene Expression Omnibus website with accession code GSE79580.

Raw reads were processed with cutadapt v.1.8.1 (https://cutadapt.readthedocs.io) to remove adapters and perform quality trimming, with default parameters except for the following: quality cutoff=20, minimum length=25 and overlap=10. Trimmed reads were mapped to the UCSC mm10 assembly using TopHat v.2.1 (Kim et al., 2013) (http://ccb.jhu.edu/software/tophat) with default parameters Reads were counted in exons of the UCSC for mm10, using feature counts (http://subread.sourceforge.net) from Subread package v.1.4.6-p3 (Liao et al., 2013). Differential expression of genes for all pairwise comparisons was assessed with DESeq2 v.1.10.1 (Love et al., 2014) (https://bioconductor.org/packages/release/bioc/html/DESeq2.html). We defined differentially regulated genes in DESeq analysis as those with adjusted $P<0.05$. Gene ontology (GO) analysis was performed using Gorilla (Eden et al., 2009) (http://cbl-gorilla.cs.technion.ac.il/).

Statistical analysis

The two-tailed Student's *t*-test was used to calculate *P*-values. Statistically significant values for $P<0.05$, $P<0.01$ and $P<0.001$ are indicated by single, double and triple asterisks, respectively.

Acknowledgements

We thank all members of Jurrien Dean's lab for helpful suggestions on the project. We thank Dr Richard Schultz (University of Pennsylvania) for providing the ZP3-pEGFP-1 plasmid, Dr Philippe Collas (University of Oslo, Norway) for providing the CMV-H3.3-eGFP and CMV-H3.3-mCherry plasmids and Dr Maria-Elena Torres Padilla (IGBMC, France) for providing the pRN3P-H3.1-GFP plasmid. We thank Dr Pawel Pelczar (University of Basel, Switzerland) for providing *Prm1*-eGFP transgenic mice. We also thank Huiyan Lu (NIDDK) for assistance on microinjection experiments.

Competing interests

The authors declare no competing or financial interests.

Author contributions

L.Z. and J.D. designed and analyzed the experiments and wrote the manuscript. L.Z. performed the experiments. L.Z. and B.B. performed microscopy analyses. B.C. performed bioinformatics analysis. L.Z. and B.X. performed microinjection experiments.

Funding

This research was support by the Intramural Research Program of the National Institute of Diabetes and Digestive and Kidney Diseases of the National Institutes of Health (DK015603-09). Deposited in PMC for release after 12 months.

Data availability

The RNA-seq dataset in this study has been deposited in Gene Expression Omnibus under accession number GSE79580 (available at: https://www.ncbi.nlm.nih.gov/geo/query/acc.cgi?acc=GSE79580).

Supplementary information

Supplementary information available online at
http://dev.biologists.org/lookup/doi/10.1242/dev.141390.supplemental

References

Akiyama, T., Suzuki, O., Matsuda, J. and Aoki, F. (2011). Dynamic replacement of histone H3 variants reprograms epigenetic marks in early mouse embryos. *PLoS Genet.* **7**, e1002279.

Aoshima, K., Inoue, E., Sawa, H. and Okada, Y. (2015). Paternal H3K4 methylation is required for minor zygotic gene activation and early mouse embryonic development. *EMBO Rep.* **16**, 803-812.

Avella, M. A., Baibakov, B. and Dean, J. (2014). A single domain of the ZP2 zona pellucida protein mediates gamete recognition in mice and humans. *J. Cell Biol.* **205**, 801-809.

Biase, F. H., Cao, X. and Zhong, S. (2014). Cell fate inclination within 2-cell and 4-cell mouse embryos revealed by single-cell RNA sequencing. *Genome Res.* **24**, 1787-1796.

Bošković, A., Eid, A., Pontabry, J., Ishiuchi, T., Spiegelhalter, C., Raghu Ram, E. V. S., Meshorer, E. and Torres-Padilla, M.-E. (2014). Higher chromatin mobility supports totipotency and precedes pluripotency in vivo. *Genes Dev.* **28**, 1042-1047.

Burkart, A. D., Xiong, B., Baibakov, B., Jiménez-Movilla, M. and Dean, J. (2012). Ovastacin, a cortical granule protease, cleaves ZP2 in the zona pellucida to prevent polyspermy. *J. Cell Biol.* **197**, 37-44.

Burton, A., Muller, J., Tu, S., Padilla-Longoria, P., Guccione, E. and Torres-Padilla, M.-E. (2013). Single-cell profiling of epigenetic modifiers identifies PRDM14 as an inducer of cell fate in the mammalian embryo. *Cell Rep.* **5**, 687-701.

Chang, C.-C., Ma, Y., Jacobs, S., Tian, X. C., Yang, X. and Rasmussen, T. P. (2005). A maternal store of macroH2A is removed from pronuclei prior to onset of somatic macroH2A expression in preimplantation embryos. *Dev. Biol.* **278**, 367-380.

Cheloufi, S., Elling, U., Hopfgartner, B., Jung, Y. L., Murn, J., Ninova, M., Hubmann, M., Badeaux, A. I., Euong Ang, C., Tenen, D. et al. (2015). The histone chaperone CAF-1 safeguards somatic cell identity. *Nature* **528**, 218-224.

Dahl, J. A., Jung, I., Aanes, H., Greggains, G. D., Manaf, A., Lerdrup, M., Li, G., Kuan, S., Li, B., Lee, A. Y. et al. (2016). Broad histone H3K4me3 domains in mouse oocytes modulate maternal-to-zygotic transition. *Nature* **537**, 548-552.

Delbarre, E., Jacobsen, B. M., Reiner, A. H., Sorensen, A. L., Kuntziger, T. and Collas, P. (2010). Chromatin environment of histone variant H3.3 revealed by quantitative imaging and genome-scale chromatin and DNA immunoprecipitation. *Mol. Biol. Cell* **21**, 1872-1884.

de Vries, W. N., Binns, L. T., Fancher, K. S., Dean, J., Moore, R., Kemler, R. and Knowles, B. B. (2000). Expression of Cre recombinase in mouse oocytes: a means to study maternal effect genes. *Genesis* **26**, 110-112.

Du, H.-N., Fingerman, I. M. and Briggs, S. D. (2008). Histone H3 K36 methylation is mediated by a trans-histone methylation pathway involving an interaction between Set2 and histone H4. *Genes Dev.* **22**, 2786-2798.

Duncan, E. M., Muratore-Schroeder, T. L., Cook, R. G., Garcia, B. A., Shabanowitz, J., Hunt, D. F. and Allis, C. D. (2008). Cathepsin L proteolytically processes histone H3 during mouse embryonic stem cell differentiation. *Cell* **135**, 284-294.

Eden, E., Navon, R., Steinfeld, I., Lipson, D. and Yakhini, Z. (2009). GOrilla: a tool for discovery and visualization of enriched GO terms in ranked gene lists. *BMC Bioinformatics* **10**, 48.

Guo, R., Zheng, L., Park, J. W., Lv, R., Chen, H., Jiao, F., Xu, W., Mu, S., Wen, H., Qiu, J. et al. (2014). BS69/ZMYND11 reads and connects histone H3.3 lysine 36 trimethylation-decorated chromatin to regulated pre-mRNA processing. *Mol. Cell* **56**, 298-310.

Hajkova, P., Jeffries, S. J., Lee, C., Miller, N., Jackson, S. P. and Surani, M. A. (2010). Genome-wide reprogramming in the mouse germ line entails the base excision repair pathway. *Science* **329**, 78-82.

Hama, H., Kurokawa, H., Kawano, H., Ando, R., Shimogori, T., Noda, H., Fukami, K., Sakaue-Sawano, A. and Miyawaki, A. (2011). Scale: a chemical approach for fluorescence imaging and reconstruction of transparent mouse brain. *Nat. Neurosci.* **14**, 1481-1488.

Haueter, S., Kawasumi, M., Asner, I., Brykczynska, U., Cinelli, P., Moisyadi, S., Bürki, K., Peters, A. H. and Pelczar, P. (2010). Genetic vasectomy-overexpression of Prm1-EGFP fusion protein in elongating spermatids causes dominant male sterility in mice. *Genesis* **48**, 151-160.

Hyland, E. M., Cosgrove, M. S., Molina, H., Wang, D., Pandey, A., Cottee, R. J. and Boeke, J. D. (2005). Insights into the role of histone H3 and histone H4 core modifiable residues in Saccharomyces cerevisiae. *Mol. Cell. Biol.* **25**, 10060-10070.

Hyllus, D., Stein, C., Schnabel, K., Schiltz, E., Imhof, A., Dou, Y., Hsieh, J. and Bauer, U.-M. (2007). PRMT6-mediated methylation of R2 in histone H3 antagonizes H3 K4 trimethylation. *Genes Dev.* **21**, 3369-3380.

Inoue, A. and Zhang, Y. (2014). Nucleosome assembly is required for nuclear pore complex assembly in mouse zygotes. *Nat. Struct. Mol. Biol.* **21**, 609-616.

Development (2017) 144, 519-528 doi:10.1242/dev.141390

Ishiuchi, T., Enriquez-Gasca, R., Mizutani, E., Bošković, A., Ziegler-Birling, C., Rodriguez-Terrones, D., Wakayama, T., Vaquerizas, J. M. and Torres-Padilla, M.-E. (2015). Early embryonic-like cells are induced by downregulating replication-dependent chromatin assembly. *Nat. Struct. Mol. Biol.* **22**, 662-671.

Jin, C. and Felsenfeld, G. (2007). Nucleosome stability mediated by histone variants H3.3 and H2A.Z. *Genes Dev.* **21**, 1519-1529.

Jullien, J., Astrand, C., Szenker, E., Garrett, N., Almouzni, G. and Gurdon, J. B. (2012). HIRA dependent H3.3 deposition is required for transcriptional reprogramming following nuclear transfer to Xenopus oocytes. *Epigenetics Chromatin* **5**, 17.

Kim, A. M., Bernhardt, M. L., Kong, B. Y., Ahn, R. W., Vogt, S., Woodruff, T. K. and O'Halloran, T. V. (2011). Zinc sparks are triggered by fertilization and facilitate cell cycle resumption in mammalian eggs. *ACS Chem. Biol.* **6**, 716-723.

Kim, D., Pertea, G., Trapnell, C., Pimentel, H., Kelley, R. and Salzberg, S. L. (2013). TopHat2: accurate alignment of transcriptomes in the presence of insertions, deletions and gene fusions. *Genome Biol.* **14**, R36.

Lewis, P. W., Muller, M. M., Koletsky, M. S., Cordero, F., Lin, S., Banaszynski, L. A., Garcia, B. A., Muir, T. W., Becher, O. J. and Allis, C. D. (2013). Inhibition of PRC2 activity by a gain-of-function H3 mutation found in pediatric glioblastoma. *Science* **340**, 857-861.

Liao, Y., Smyth, G. K. and Shi, W. (2013). The Subread aligner: fast, accurate and scalable read mapping by seed-and-vote. *Nucleic Acids Res.* **41**, e108.

Lin, C.-J., Conti, M. and Ramalho-Santos, M. (2013). Histone variant H3.3 maintains a decondensed chromatin state essential for mouse preimplantation development. *Development* **140**, 3624-3634.

Lin, C.-J., Koh, F. M., Wong, P., Conti, M. and Ramalho-Santos, M. (2014a). Hira-mediated H3.3 incorporation is required for DNA replication and ribosomal RNA transcription in the mouse zygote. *Dev. Cell* **30**, 268-279.

Lin, R.-S., Jimenez-Movilla, M. and Dean, J. (2014b). Figla-Cre transgenic mice expressing myristoylated EGFP in germ cells provide a model for investigating perinatal oocyte dynamics. *PLoS ONE* **9**, e84477.

Liu, C.-P., Xiong, C., Wang, M., Yu, Z., Yang, N., Chen, P., Zhang, Z., Li, G. and Xu, R.-M. (2012). Structure of the variant histone H3.3-H4 heterodimer in complex with its chaperone DAXX. *Nat. Struct. Mol. Biol.* **19**, 1287-1292.

Liu, X., Wang, C., Liu, W., Li, J., Li, C., Kou, X., Chen, J., Zhao, Y., Gao, H., Wang, H. et al. (2016). Distinct features of H3K4me3 and H3K27me3 chromatin domains in pre-implantation embryos. *Nature* **537**, 558-562.

Love, M. I., Huber, W. and Anders, S. (2014). Moderated estimation of fold change and dispersion for RNA-seq data with DESeq2. *Genome Biol.* **15**, 550.

Lu, F., Liu, Y., Inoue, A., Suzuki, T., Zhao, K. and Zhang, Y. (2016). Establishing chromatin regulatory landscape during mouse preimplantation development. *Cell* **165**, 1375-1388.

Macfarlan, T. S., Gifford, W. D., Driscoll, S., Lettieri, K., Rowe, H. M., Bonanomi, D., Firth, A., Singer, O., Trono, D. and Pfaff, S. L. (2012). Embryonic stem cell potency fluctuates with endogenous retrovirus activity. *Nature* **487**, 57-63.

Nashun, B., Hill, P. W. S., Smallwood, S. A., Dharmalingam, G., Amouroux, R., Clark, S. J., Sharma, V., Ndjetehe, E., Pelczar, P., Festenstein, R. J. et al. (2015). Continuous histone replacement by hira is essential for normal transcriptional regulation and de novo DNA methylation during mouse oogenesis. *Mol. Cell* **60**, 611-625.

Plachta, N., Bollenbach, T., Pease, S., Fraser, S. E. and Pantazis, P. (2011). Oct4 kinetics predict cell lineage patterning in the early mammalian embryo. *Nat. Cell Biol.* **13**, 117-123.

Que, E. L., Bleher, R., Duncan, F. E., Kong, B. Y., Gleber, S. C., Vogt, S., Chen, S., Garwin, S. A., Bayer, A. R., Dravid, V. P. et al. (2015). Quantitative mapping of zinc fluxes in the mammalian egg reveals the origin of fertilization-induced zinc sparks. *Nat. Chem.* **7**, 130-139.

Rinkevich, Y., Lindau, P., Ueno, H., Longaker, M. T. and Weissman, I. L. (2011). Germ-layer and lineage-restricted stem/progenitors regenerate the mouse digit tip. *Nature* **476**, 409-413.

Santenard, A., Ziegler-Birling, C., Koch, M., Tora, L., Bannister, A. J. and Torres-Padilla, M.-E. (2010). Heterochromatin formation in the mouse embryo requires critical residues of the histone variant H3.3. *Nat. Cell Biol.* **12**, 853-862.

Schwartzentruber, J., Korshunov, A., Liu, X.-Y., Jones, D. T. W., Pfaff, E., Jacob, K., Sturm, D., Fontebasso, A. M., Quang, D. A., Tonjes, M. et al. (2012). Driver mutations in histone H3.3 and chromatin remodelling genes in paediatric glioblastoma. *Nature* **482**, 226-231.

Shi, J., Chen, Q., Li, X., Zheng, X., Zhang, Y., Qiao, J., Tang, F., Tao, Y., Zhou, Q. and Duan, E. (2015). Dynamic transcriptional symmetry-breaking in pre-implantation mammalian embryo development revealed by single-cell RNA-seq. *Development* **142**, 3468-3477.

Stewart, K. R., Veselovska, L., Kim, J., Huang, J., Saadeh, H., Tomizawa, S.-i., Smallwood, S. A., Chen, T. and Kelsey, G. (2015). Dynamic changes in histone modifications precede de novo DNA methylation in oocytes. *Genes Dev.* **29**, 2449-2462.

Svoboda, P., Stein, P. and Schultz, R. M. (2001). RNAi in mouse oocytes and preimplantation embryos: effectiveness of hairpin dsRNA. *Biochem. Biophys. Res. Commun.* **287**, 1099-1104.

Tabansky, I., Lenarcic, A., Draft, R. W., Loulier, K., Keskin, D. B., Rosains, J., Rivera-Feliciano, J., Lichtman, J. W., Livet, J., Stern, J. N. H. et al. (2013). Developmental bias in cleavage-stage mouse blastomeres. *Curr. Biol.* **23**, 21-31.

Tang, F., Barbacioru, C., Nordman, E., Bao, S., Lee, C., Wang, X., Tuch, B. B., Heard, E., Lao, K. and Surani, M. A. (2011). Deterministic and stochastic allele specific gene expression in single mouse blastomeres. *PLoS ONE* **6**, e21208.

Tang, M. C. W., Jacobs, S. A., Mattiske, D. M., Soh, Y. M., Graham, A. N., Tran, A., Lim, S. L., Hudson, D. F., Kalitsis, P., O'Bryan, M. K. et al. (2015). Contribution of the two genes encoding histone variant h3.3 to viability and fertility in mice. *PLoS Genet.* **11**, e1004964.

Torres-Padilla, M. E., Bannister, A. J., Hurd, P. J., Kouzarides, T. and Zernicka-Goetz, M. (2006). Dynamic distribution of the replacement histone variant H3.3 in the mouse oocyte and preimplantation embryos. *Int. J. Dev. Biol.* **50**, 455-461.

Torres-Padilla, M. E., Parfitt, D. E., Kouzarides, T. and Zernicka-Goetz, M. (2007). Histone arginine methylation regulates pluripotency in the early mouse embryo. *Nature* **445**, 214-218.

Wen, D., Banaszynski, L. A., Liu, Y., Geng, F., Noh, K.-M., Xiang, J., Elemento, O., Rosenwaks, Z., Allis, C. D. and Rafii, S. (2014a). Histone variant H3.3 is an essential maternal factor for oocyte reprogramming. *Proc. Natl. Acad. Sci. USA* **111**, 7325-7330.

Wen, H., Li, Y., Xi, Y., Jiang, S., Stratton, S., Peng, D., Tanaka, K., Ren, Y., Xia, Z., Wu, J. et al. (2014b). ZMYND11 links histone H3.3K36me3 to transcription elongation and tumour suppression. *Nature* **508**, 263-268.

White, M. D., Angiolini, J. F., Alvarez, Y. D., Kaur, G., Zhao, Z. W., Mocskos, E., Bruno, L., Bissiere, S., Levi, V. and Plachta, N. (2016). Long-lived binding of Sox2 to DNA predicts cell fate in the four-cell mouse embryo. *Cell* **165**, 75-87.

Wu, J., Huang, B., Chen, H., Yin, Q., Liu, Y., Xiang, Y., Zhang, B., Liu, B., Wang, Q., Xia, W. et al. (2016). The landscape of accessible chromatin in mammalian preimplantation embryos. *Nature* **534**, 652-657.

Zheng, P. and Dean, J. (2009). Role of Filia, a maternal effect gene, in maintaining euploidy during cleavage-stage mouse embryogenesis. *Proc. Natl. Acad. Sci. USA* **106**, 7473-7478.

Zhou, L. q. and Dean, J. (2015). Reprogramming the genome to totipotency in mouse embryos. *Trends Cell Biol.* **25**, 82-91.

Ziegler-Birling, C., Daujat, S., Schneider, R. and Torres-Padilla, M.-E. (2016). Dynamics of histone H3 acetylation in the nucleosome core during mouse pre-implantation development. *Epigenetics* **11**, 553-562.

SUPPLEMENTARY FIGURES

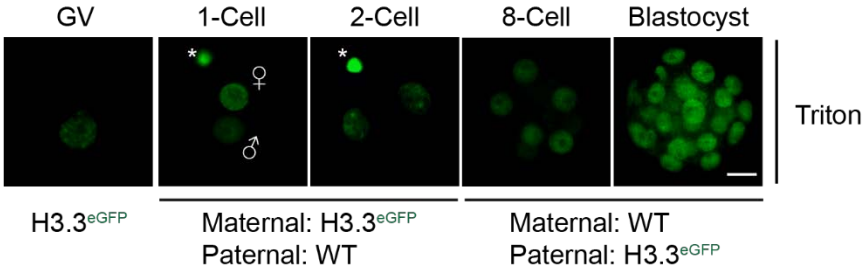

Fig. S1. H3.3 is consistently incorporated into parental chromatin in oocytes and embryos. Confocal imaging (full projection) of GV oocytes and early embryos (1C to blastocyst) expressing eGFP-tagged H3.3 with indicated genotypes. Oocytes and embryos were collected and treated with 0.5% Triton for 10 min before fixation for imaging, in order to remove any non-chromatin bound proteins. Asterisk, polar bodies; scale bar, 20 μm.

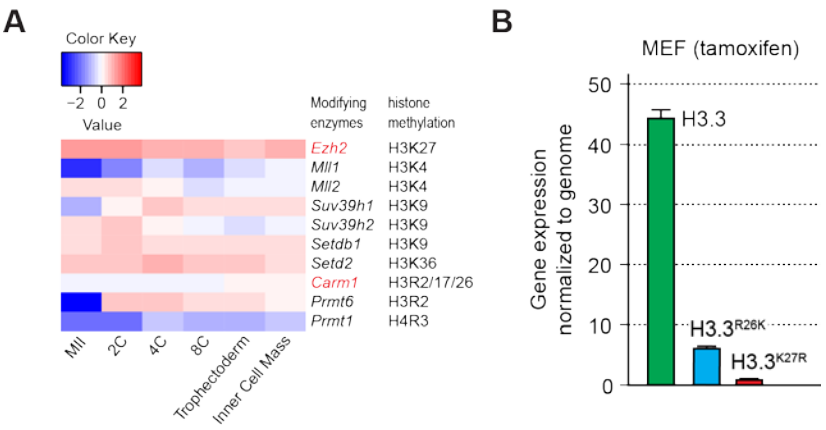

Fig. S2. Selection of R26 and K27 for mutation to construct Rainbow cassette. (A) Heatmap for transcript abundance of histone modifying enzymes during preimplantation development. Color code for expression level (Z-score normalized $\log_2$ RPM value). Enzymes modifying K27 or R26 are indicated in red. (B) Recombination efficiency was quantified in transgenic HISRainbow;CreER MEF cells (n =3 cell lines from 3 mice) 2 days after induction with 1 μM 4-hydroxytamoxifen. Gene expression was determined by realtime RT-PCR and expression of $H3.3^{K27R}$ was set as 1. Mean ± s.e.m.

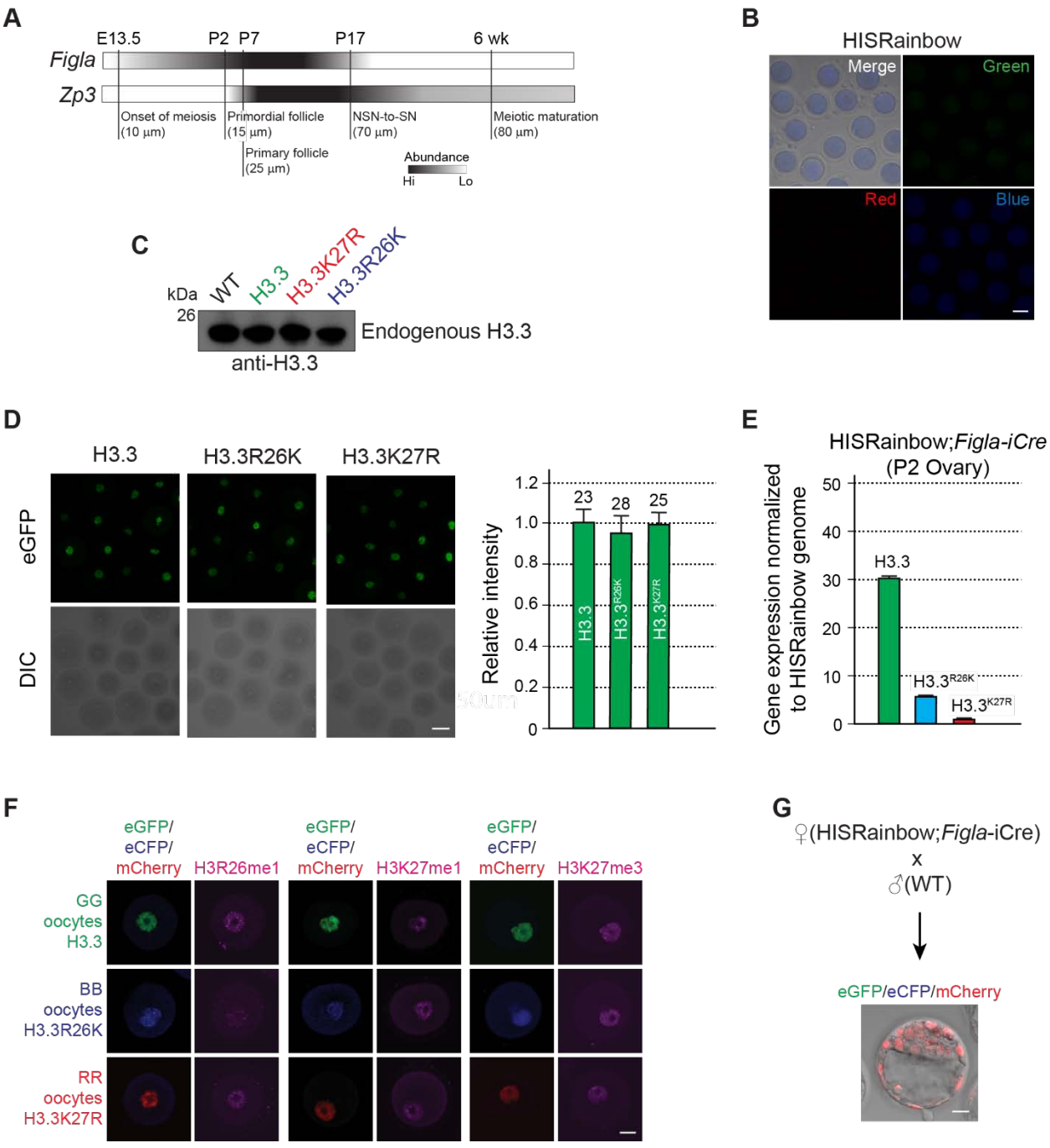

Fig. S3. Recombination of the HISRainbow cassette in oocytes. (A) Timelines of *Figla* and *Zp3* expression beginning with the onset of meiosis at E13.5 and continuing through folliculogenesis to fully grown, meiotically mature oocytes. Activation of the *Figla* promoter begins at meiosis and peaks in primordial follicles. Activation of the *Zp3* promoter begins in primary follicles and extends through the 2-week growth phase of

folliculogenesis. E, embryonic day; P, post-natal day. (B) Confocal (full projection) and DIC images of MII oocytes isolated from HISRainbow female mice. No fluorescent signals were observed. Scale bar, 50 μm. (C) Immunoblot analysis of HISRainbow;*Figla*-iCre GV oocytes with indicated genotypes for endogenous H3.3 expression. 25 oocytes were collected for each group: WT, H3.3^{eGFP} (GG), H3.3K27R^{mCherry} (RR) and H3.3R26K^{eCFP} (BB) and loaded into each lane. Representative gel of 2 experiments. (D) cRNAs encoding H3.3^{eGFP}, H3.3R26K^{eGFP} and H3.3K27R^{eGFP} were injected into GV oocytes. Oocytes were incubated at 37 °C in KSOM with 2.5 μM milrinone for 24 hr and fixed for imaging (left). Fluorescent signals were then quantified for 23-28 oocytes in each group and fluorescent intensity from H3.3^{eGFP} group was set as 1 (right). (E) Recombination efficiency was quantified in P2 HISRainbow;*Figla*-iCre ovaries (n =6 mice) by RT-PCR and expression of H3.3^{K27R} was set as 1. Mean ± s.e.m. (F) Immunofluorescence of histone modifications (H3R26me1, H3K27me1, H3K27me3) in HISRainbow;*Figla*-iCre oocytes. Scale bar, 20 μm. (G) HISRainbow;*Figla*-iCre female were mated with WT male mice. 1C zygotes were collected and cultured to the blastocyst stage. Confocal (full projection) image of a representative blastocyst expressing H3.3K27R^{mCherry}. Asterisk, polar body; scale bar, 20 μm.

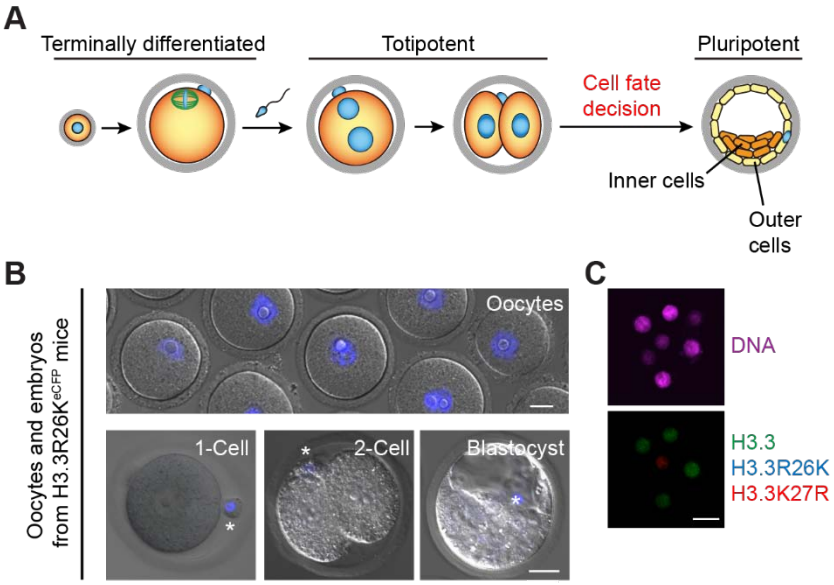

Fig. S4. Expression of H3.3 mutants in early mouse embryos. (A) Scheme of cell lineage specification in early mouse embryos. (B) GV oocytes were isolated from H3.3R26K^{eCFP} transgenic females. H3.3R26K transgenic females were mated with WT males, followed by zygote collection and culturing in KSOM until blastocyst stage. No eCFP signal was detectable in nuclei of embryos. Asterisk, polar body; scale bar, 20 μm. (C) Representative confocal (full projection) image of the mosaic embryo at 8-16-cell stage with individual blastomeres expressing either H3.3^{eGFP} or H3.3K27R^{mCherry}. DNA was stained by DRAQ5. Scale bar, 20 μm.

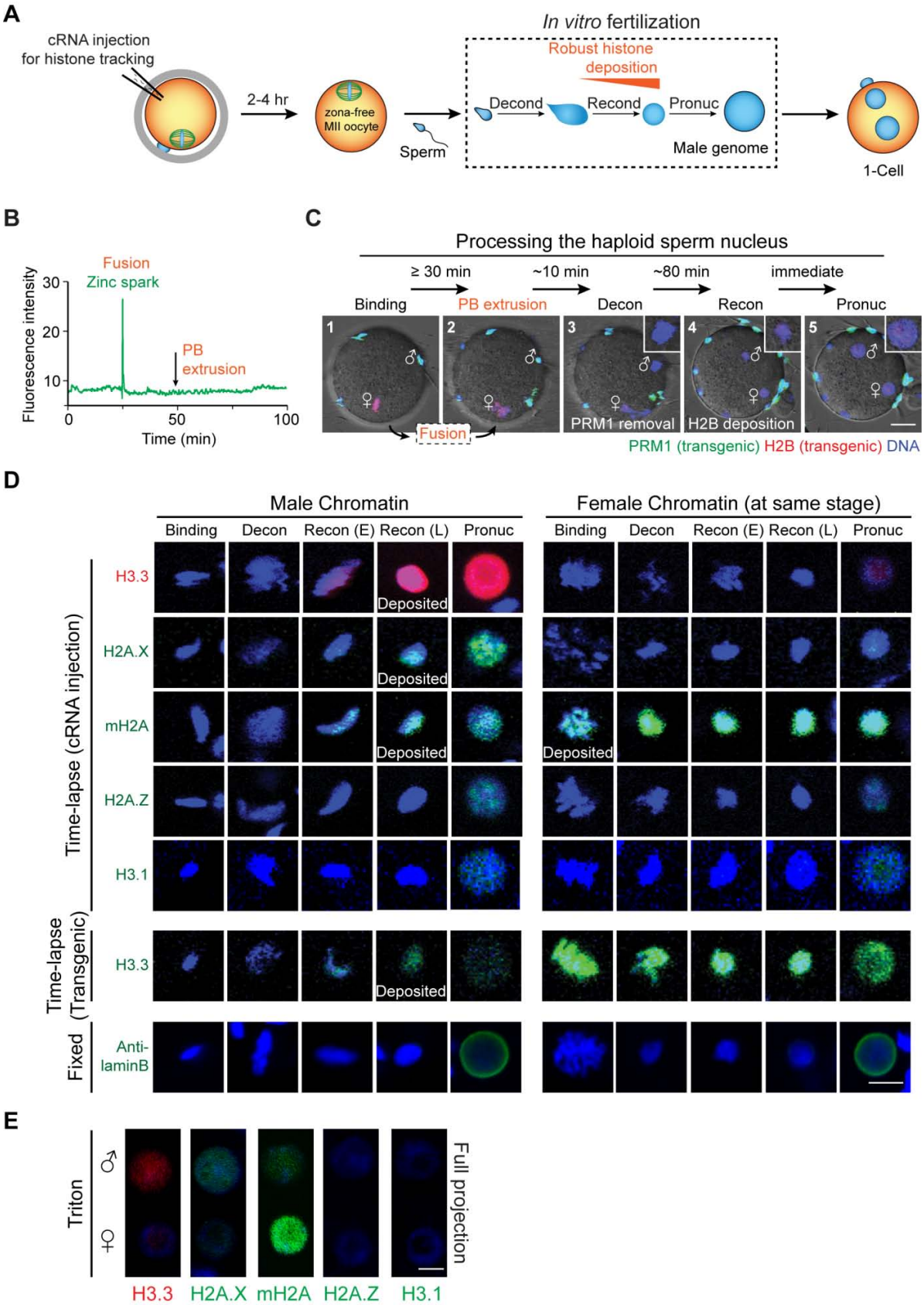

Fig. S5. Imaging parental genome reorganization during the protamine-to-histone exchange. (A) Histones with fluorescent tags can be imaged during fertilization to monitor their dynamics. (B) Sperm-oocyte fusion was determined by imaging zinc sparks with FluoZin-3. (C) Sperm expressing eGFP-tagged Protamine 1 (PRM1) and oocytes expressing mCherry-tagged H2B were imaged to track protamine removal and histone deposition, respectively, with representative images of 10 zygotes shown. 1, sperm-oocyte binding (Binding); 2, polar body (PB) extrusion; 3, male genome de-condensation (Decon); 4, re-condensation (Recon); 5, pronuclei formation (Pronuc). Insets in panels 3-5 are 2X magnification of the male genome. Approximate time between each step is indicated above. Scale bar, 20 μm. (D) For imaging during *in vitro* fertilization, either cRNAs encoding eGFP or mCherry-tagged histone variants (indicated by green or red color) were microinjected into MII oocytes, or MII oocytes were directly collected from hormonally stimulated transgenic female. Images of individual steps of male genome reorganization are shown. Early and late phases of re-condensation are indicated with E and L. To confirm nuclear membrane formation during this process, we collected zygotes every two hr until six hr, performed Triton treatment and paraformaldehyde fixation, stained with anti-lamin B antibody, and documented that pronuclei with nuclear membrane are formed after Recon (L). 6-10 zygotes have been imaged for each group with a representative image displayed. Scale bar, 10 μm. (E) To confirm histone variant association, MII oocytes were injected, fertilized by WT sperm and collected at the early 1-cell stage for treatment with 0.5% Triton (10 min), followed by fixation and imaging. 10-15 zygotes were imaged for each group with a representative image displayed. Scale bar, 10 μm.

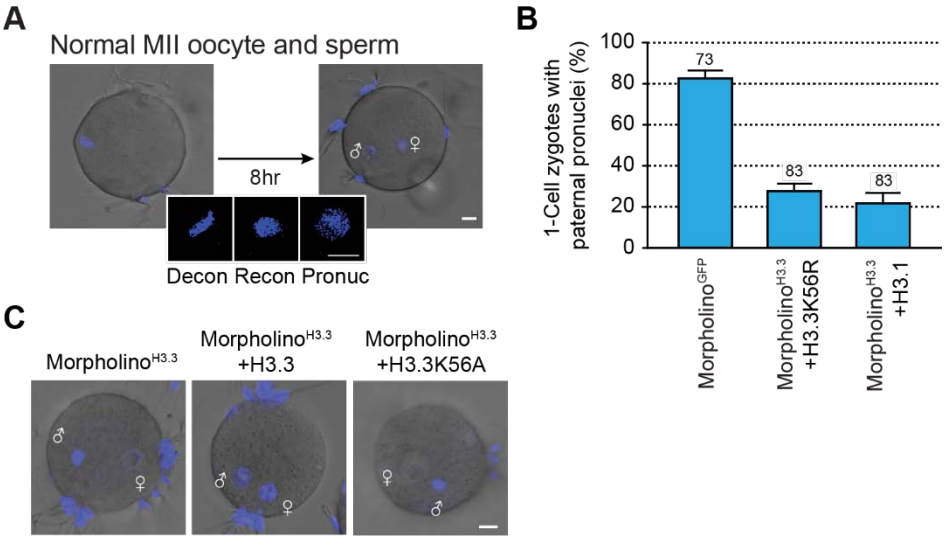

Fig. S6. H3.3K56 is essential for male pronuclei formation. (A) Representative merged DIC and fluorescent images of WT sperm progressing sequentially from de-condensation (Decond) to re-condensation (Recond) to pronucleus formation (Pronuc) after fusion with the *in vitro* matured MII oocyte (23 oocytes were imaged). (B) GV oocytes were injected with morpholinos and cRNA as indicated for *in vitro* maturation (18 hr) and *in vitro* fertilization. Oocytes, matured and fertilized *in vitro*, were fixed and observed 8 hr after insemination. Formation of paternal pronuclei was determined morphologically in fertilized oocytes treated with and without morpholinos (n =73-83). (C) Representative images of endogenous H3.3 deplete zygotes (left) rescued with cRNA encoding H3.3 WT (middle) or H3.3K56A (right). Scale bar, 10 μm.

Table S1. Primers.

	Mouse line/gene name	Primer sequence (forward, reverse)	PCR product (size)
Genotype	HISRainbow pCAG-H3.3^{eGFP}	CCAATCTGTGCGCCATTCAC ACATGAACTGAGGGGACAGG	327 bp
	ZP3-H2B^{mCherry}	CCGACTACTTGAAGCTGTCCTT CATGGTCTTCTTCTGCATTACG	185 bp
Tag discrimination	eGFP	TCGTGACCACCCTGACCTAC CTGCTTGTCGGCCATGATAT	293 bp
	eCFP	CGTGACCACCCTGACCTGG GTTCTTCTGCTTGTCGGCGG	298 bp
	mCherry	CCGACTACTTGAAGCTGTCCTT CATGGTCTTCTTCTGCATTACG	185 bp
	H33XFPUTR	CAATCTGTGCGCCATTCAC TGTTGCCAAACTCTAAACCAA	1116 bp

Table S2. Distribution of subpopulations in oocytes.

Genotype	GG[1]	BB	RR	GB	GR	BR	Total
HISRainbow; *Figla*-iCre[3] (P2 Ovary, n =6 mice)	67.83 ± 1.87[2]	2.29 ± 0.28	0.09 ± 0.03	24.54 ± 1.31	4.44 ± 0.74	0.82 ± 0.17	100
HISRainbow; *Figla*-iCre (n =7 mice)	9.18 ± 2.91	9.73 ± 2.84	22.43 ± 2.89	18.36 ± 1.86	16.69 ± 2.33	23.61 ± 3.35	100
HISRainbow; *ZP3*-Cre (n =8 mice)	8.15 ± 2.38	8.08 ± 1.95	19.95 ± 2.79	20.99 ± 4.16	21.78 ± 2.79	21.04 ± 3.48	100

[1]G indicates H3.3, B indicates $H3.3^{R26K}$, R indicates $H3.3^{K27R}$.

[2]Data is displayed in percentage ± s.e.m; n, number of mice analyzed.

[3]Subpopulation distributions in P2 ovary were calculated from the percentages of total H3.3 (G^{total}), total $H3.3^{R26K}$ (B^{total}), and total $H3.3^{K27R}$ (R^{total}) transcripts expressed from the HISRainbow cassette (Fig. S3C): GG =$(G^{total})^2$, BB =$(B^{total})^2$, RR =$(R^{total})^2$, GB =$2(G^{total})(B^{total})$, GR =$2(G^{total})(R^{total})$, BR =$2(B^{total})(R^{total})$.

Table S3. Distribution of blastomeres expressing H3.3^{eGFP} (G) and H3.3K27R^{mCherry} (R) in early blastocysts (HISRainbow;CreER).

H3.3 Isoform	Inner cells	Outer cells	Total
G	30.24 ± 1.17[1]	69.76 ± 1.17	100
R	19.23 ± 3.09	80.77 ± 3.09	100

[1]Data is displayed in percentage ± s.e.m of 30 blastocysts.

Blastocysts	Inner cells (G)	Outer cells (G)	Inner cells (R)	Outer cells (R)
1	4[2]	13	0	2
2	4	9	1	5
3	6	14	1	3
4	5	11	1	5
5	8	19	0	2
6	3	8	0	1
7	6	11	0	4
8	4	10	2	2
9	5	10	0	2
10	1	5	0	1
11	3	7	1	2
12	3	6	1	5
13	5	13	1	2
14	3	8	2	2
15	4	6	2	3
16	3	8	0	3
17	4	6	0	3
18	2	7	2	3
19	5	8	2	5
20	4	9	2	6
21	3	11	1	3
22	3	7	0	2
23	2	8	0	2
24	8	10	2	4
25	5	9	1	2
26	2	4	1	4
27	2	7	2	3
28	4	9	0	2
29	3	8	1	3
30	5	8	1	3
Total	119	269	27	89

[2]Data is displayed as cell number in blastocyst.

Table S4. Distribution of blastomeres expressing H3.3^{eGFP} (G) and H3.3K27R^{mCherry} (R) in 8-16-cell embryos (HISRainbow;CreER).

Embryo	G	R
1	4[1]	1
2	4	2
3	3	2
4	3	1
5	4	2
6	5	1
7	5	2
8	4	1
9	6	1
10	5	2
11	5	1
12	4	1
13	6	2
14	4	2
15	5	1
16	4	2
17	6	2
18	5	1
Total	82	27

[1]Data is displayed as cell number in embryos.